Time-energy consumption optimal path-constrained trajectory planning of excavator robotics

Yunyue Zhang[1] Zhiyi Sun[1] Qianlai Sun[1] Yin Wang[1]

[1]School of Electronic and Information Engineering, Taiyuan University of Science and Technology, Taiyuan 030024, China

Abstract

During the cyclic operation process of hydraulic excavators, based on manual experience, issues such as low work efficiency and high energy consumption can cause significantly high wearing of the joints of the excavator; this markedly affects the service life of the excavator. To solve such issues, we propose a secondary trajectory optimization method based on time–energy consumption that enables the excavator to conduct smooth, efficient, and low-energy-consumption work. Considering different weight coefficient values and obtaining the optimal time–energy trajectory, we compare the above-mentioned results with those obtained through skilled manual operation of hydraulic excavators. The experimental results demonstrate that through reasonable and effective planning of each joint movement, the large jerk that occurs during joint movement processes may be effectively avoided, the working efficiency of the excavator is improved, unnecessary energy consumption is reduced, and the excavator can operate autonomously under stable conditions. These results verify the effectiveness and feasibility of the proposed method.

Keywords

Cubic spline; Excavator robotics; Convex optimization; Time–energy consumption; Trajectory planning

1. INTRODUCTION

Hydraulic excavators are indispensable mechanical equipment for numerous engineering applications. They are extensively used for complex excavation and under harsh working conditions, such as during earthquake relief, in space, and for underwater operations [1-3]. Owing to the complexity of these working environments, the safety of staff members can be threatened and improper operation may lead to problems such as high energy consumption and mechanical wear, resulting in equipment damage and a reduction in the service life of the excavator [4-6]. Consequently, with the development of science technology, and artificial intelligence, intelligent and automated excavators are gradually emerging.

Autonomous excavators can not only avoid humans from entering the dangerous working environment, but also provide guarantees for the realization of difficult tasks, and give full play to the value of excavators in engineering applications [7,8]. Therefore, scholars have carried out in-depth research on intelligent excavators in recent years. Among them, in the many intelligent technologies of excavators, the operation trajectory, as the premise and foundation of the excavator's autonomous working, directly affects the work efficiency and energy consumption of the excavator. Therefore, it is of great significance to carry out

[1]Corresponding author:
Zhiyi Sun, School of Electronic and Information Engineering, Taiyuan University of Science and Technology, Taiyuan 030024, China.
E-mail: 1020596674@qq.com.

effective and reasonable planning of the trajectory [9,10].

Currently, with the continuous expansion of the scope of application of intelligent optimization algorithms, Huang et al.[11] used the non-dominated sorting genetic algorithm (NSGA-II) to optimize and solve the multi-objective time-jerk optimal trajectory. Kucuk [12,13] optimized and solved the smooth seventh-order polynomial optimal time trajectory using the particle swarm optimization algorithm (PSO). Furthermore, to achieve smoothness, high efficiency, and low energy consumption operations of large-scale equipment, [14,16] simultaneously considered time and energy problems and obtained an optimal trajectory that satisfies multiple goals. However, due to common problems, such as slow convergence speeds and poor local exploration abilities in intelligent algorithms, the optimal solution obtained may the local optimal solution.

And [17,18] used dynamic programming to obtain time-optimal trajectories under multiple constraints. They achieved high-efficiency working trajectory planning relative to other methods, but obtaining the optimal solution requires long computation times.

In optimal trajectory planning research work using numerical analysis, the phase plane [19,23] which is a maximum pseudo-velocity curve is derived according to the torque constraint conditions to obtain the time-optimal trajectory. Liu et al. [24] transformed the optimal energy consumption problem into the ternary functional extreme value problem, solving the Euler equation using a combination of the fourth-order Runge-Kutta method and the multiple shooting method. But the above approaches are suitable only for solving single-objective optimal trajectory planning problems and cannot solve optimal trajectory planning for multiple objectives.

For the problems existing in the above research, as an efficient iterative algorithm for solving nonlinear convex optimization problems, the interior-point method not only has a wide range of applications but also has high computational efficiency. It searches for the optimal solution by traversing the internal feasible region. Therefore, the present study uses the PC1012 hydraulic excavator robot as its research object, proposing secondary trajectory optimization with time-energy consumption as the optimization objective under the constraints of velocity, acceleration, and jerk. By introducing a pseudo-path parameter s, the optimization objective function and constraints may be transformed into a convex optimization model. According to the secondary planning of the hydraulic excavator along the given lifting path, the convex optimization method, i.e., the interior-point method, is then used to optimize the time-energy trajectory. The results show that the secondary optimized trajectories improve the motion efficiency of each joint, reduce energy loss, and achieve the smooth movement of the excavator.

The main contributions of this paper are summarized as follows:

1) To improve the efficiency of the secondary working path of the excavator and reduce its energy consumption, the trajectory planning with time-energy consumption as the optimization objective is proposed.

2) To achieve a smooth planned trajectory, an equivalent convex jerk constraint is established considering the conditions of the pseudo-path velocity and acceleration constraints.

3) The interior-point method is used to optimize the time-energy consumption optimal trajectory under the constraints of joint velocity, acceleration, and jerk.

4) The PC1012 hydraulic excavator is used for experiments to verify the effectiveness and feasibility of the proposed planning method.

This paper is structured as follows. Section 2 introduces the expression of the nonlinear coupled dynamics model of the pseudo-path parameter s. Section 3 presents the formulation of the time–energy

optimal trajectory planning problem and its kinematics and dynamics constraints. Section 4 describes the specific solution process of the optimization problem. Section 5 discusses experimental simulation results using the PC1012 hydraulic excavator robotics. Section 6 presents the conclusions.

2. DYNAMICS ANALYSIS

The dynamic model expression of the hydraulic excavator robotic working device is shown in equation (1). The functional relational expression of the torque concerns each joint angle, velocity, and acceleration.

$$\boldsymbol{\tau} = \boldsymbol{M}(\boldsymbol{q})\ddot{\boldsymbol{q}} + \boldsymbol{C}(\boldsymbol{q},\dot{\boldsymbol{q}})\dot{\boldsymbol{q}} + \boldsymbol{g}(\boldsymbol{q}) \tag{1}$$

where $\boldsymbol{q} \in \boldsymbol{R}^3, \dot{\boldsymbol{q}} \in \boldsymbol{R}^3, \ddot{\boldsymbol{q}} \in \boldsymbol{R}^3$ represent the joint angle, velocity, and acceleration vector, respectively, in which $\dot{q}$ and $\ddot{q}$ are the first and second derivatives of the joint displacement q with respect to time t. $\boldsymbol{M}(\boldsymbol{q}) \in \boldsymbol{R}^{3*3}$ is the inertia matrix, $\boldsymbol{C}(\boldsymbol{q},\dot{\boldsymbol{q}}) \in \boldsymbol{R}^{3*3}$ is the Coriolis force and the centrifugal force matrix, $\boldsymbol{g}(\boldsymbol{q}) \in \boldsymbol{R}^{3*1}$ is the torque vector caused by gravity, and $\boldsymbol{\tau} \in \boldsymbol{R}^{3*1}$ represents the driving torque of each joint.

To solve equation (1), by applying the kinematics inverse solution to the discrete points of the target trajectory in the workspace, the angle value sequence of the boom, arm, and bucket joint can be obtained. However, the velocity and acceleration along the given path, as well as the time for completing the task, are unknown. And the derivatives of q concerning time cannot be calculated.

Therefore, a normalized and monotonically increasing pseudo-path parameter s is introduced to obtain the velocity and acceleration of each joint with path parameter s, where the path in the joint space is represented by $q(s)$. The time parameterization of the target path is expressed as $s(t)$, $t \in [0,T]$, where T is the total movement time required to complete the target trajectory, which satisfies $s(0) = 0 \le s(t) \le 1 = s(T)$, $\dot{s}(t) > 0$. $q(s(0)) = q(0)$ is the joint position of the initial point of the target path, and $q(s(T)) = q(1)$ is the joint position corresponding to the endpoint of the path. As mentioned before, the joint velocity, acceleration, and jerk are defined by pseudo-path parameters s as follows:

$$\dot{\boldsymbol{q}}(s) = \boldsymbol{q}'(s)\dot{s} \tag{2}$$

$$\ddot{\boldsymbol{q}}(s) = \boldsymbol{q}'(s)\ddot{s} + \boldsymbol{q}''(s)\dot{s}^2 \tag{3}$$

$$\dddot{\boldsymbol{q}}(s) = 3\boldsymbol{q}''(s)\ddot{s} + \boldsymbol{q}'(s)\dddot{s} + \boldsymbol{q}'''(s)\dot{s}^2 \tag{4}$$

where $\dot{s} = ds/dt$, $\dot{s}$ represents the velocity of the pseudo-path; $\ddot{s} = d^2s/dt^2$, $\ddot{s}$ is the acceleration of the pseudo-path; $\dddot{s} = d^3s/dt^3$, $\dddot{s}$ is the jerk of the pseudo-path.

$\boldsymbol{q}'(s) = \partial \boldsymbol{q}(s)/\partial s, \boldsymbol{q}''(s) = \partial^2 \boldsymbol{q}(s)/\partial s^2, \boldsymbol{q}'''(s) = \partial^3 \boldsymbol{q}(s)/\partial s^3$ respectively represents the derivative of $\boldsymbol{q}(s)$ with respect to the variable s. Substituting equations (2-3) into equation (1), the dynamical model with pseudo-path parameter s, as well as their variables derivatives $\dot{s}, \ddot{s}$ can be obtained, as shown in equation (5).

$$\boldsymbol{\tau}(s) = \boldsymbol{m}(s)\ddot{s} + \boldsymbol{c}(s)\dot{s}^2 + \boldsymbol{g}(s) \tag{5}$$

where $\boldsymbol{m}(s) = \boldsymbol{M}(\boldsymbol{q}(s))\boldsymbol{q}'(s)$, $\boldsymbol{c}(s) = \boldsymbol{M}(\boldsymbol{q}(s))\boldsymbol{q}''(s) + \boldsymbol{C}(\boldsymbol{q}(s),\boldsymbol{q}'(s))\boldsymbol{q}'(s)$, $\boldsymbol{g}(s) = \boldsymbol{G}(\boldsymbol{q}(s))$. Among them, by discretizing the given target trajectory, the discrete angle sequence values of each joint are fitted by cubic spline, and the value of $\boldsymbol{m}(s), \boldsymbol{c}(s), \boldsymbol{g}(s)$ can be calculated using the cubic spline fitting curve $\boldsymbol{q}(s)$.

3. CONVEX PROBLEM MODEL

3.1 The time–energy optimal problem

To realize the efficient and low-energy operation of the excavator, an objective function is established with time and energy consumption as the optimization object, as shown in equations (6-7).

$$\min T = \int_0^T 1dt = \int_{s(0)}^{s(T)} \frac{dt}{ds} * ds = \int_0^1 \frac{1}{\dot{s}} ds \tag{6}$$

$$\min \int_0^T \tau_i(s)^2 dt = \int_0^1 \frac{\tau_i(s)^2}{\dot{s}} ds \tag{7}$$

Combining equation (5), the objective function is to optimize the problem of solving pseudo-velocity squared $\dot{s}^2$ and pseudo-acceleration $\ddot{s}$. Defining the optimization variable as $l(s) = \ddot{s}, u(s) = \dot{s}^2$, the constraint condition is obtained as follows.

$$u'(s) = \frac{d\dot{s}^2}{ds} = 2\dot{s}\frac{d\dot{s}}{dt}\frac{dt}{ds} = 2\ddot{s} \Leftrightarrow u'(s) = 2l(s) \tag{8}$$

Considering the safety performance of the excavator, the velocity and acceleration of each joint at the start and endpoints are zero, that is $u(0) = \dot{s}_0{}^2 = 0$, $u(1) = \dot{s}_T{}^2 = 0$, $l(0) = \ddot{s}_0 = 0$, and $l(1) = \ddot{s}_T = 0$. According to the above derivation, the objective functions of equations (6-7) are transformed into the following form

$$\min_{l(\bullet),u(\bullet),\boldsymbol{\tau}(\bullet)} \int_0^1 \eta_1 \frac{1}{\sqrt{u(s)}} ds + (1-\eta_1) \int_0^1 \frac{\tau_i(s)^2}{\sqrt{u(s)}} ds, \tag{9}$$

subject to

$$\boldsymbol{\tau}_i(s) = \boldsymbol{m}_i(s)l(s) + \boldsymbol{c}_i(s)u(s) + \boldsymbol{g}_i(s), \tag{10}$$

$$u(0) = 0, \quad u(1) = 0, \tag{11}$$

$$l(0) = 0, \quad l(1) = 0, \tag{12}$$

$$u'(s) = 2l(s), \ u(s) \geq 0, \tag{13}$$

$$\boldsymbol{\tau}_{i\min}(s) \leq \boldsymbol{\tau}(s) \leq \boldsymbol{\tau}_{i\max}(s), \tag{14}$$

where $i = 1, 2, 3$ correspond to boom, arm, and bucket joints respectively, and η_1 is the weight coefficient, $0 \leq \eta_1 \leq 1$.

3.2 Inequality constraints condition

In addition to considering the torque constraints, considering the path constraints of velocity, acceleration and jerk are also necessary. For $i-th$ joint, the process of converting joint velocity constraint into path velocity constraint is shown in equation (15).

$$\begin{aligned} &-\dot{q}_{i\max}(s) \leq \dot{q}_i(s) \leq \dot{q}_{i\max}(s) \\ &\Leftrightarrow -\dot{q}_{i\max}(s) \leq q'_i(s)\dot{s} \leq \dot{q}_{i\max}(s) \\ &\Leftrightarrow (q'_i(s)\dot{s})^2 = (q'_i(s))^2 u(s) \leq (\dot{q}_{i\max}(s))^2 \\ &\Leftrightarrow u(s) \leq (\dot{q}_{i\max}(s))^2 / (q'_i(s))^2 \end{aligned} \tag{15}$$

The established path acceleration constraint condition is shown in equation (16).

$$\begin{aligned} &-\ddot{q}_{i\max}(s) \leq \ddot{q}_i(s) \leq \ddot{q}_{i\max}(s) \Leftrightarrow -\ddot{q}_{i\max}(s) \leq q_i'(s)\ddot{s} + q_i''(s)\dot{s}^2 \leq \ddot{q}_{i\max}(s) \\ &\Leftrightarrow -\ddot{q}_{i\max}(s) \leq q_i'(s)l(s) + q_i''(s)u(s) \leq \ddot{q}_{i\max}(s) \\ &\Leftrightarrow \frac{-\ddot{q}_{i\max}(s) - q_i''(s)u(s)}{q_i'(s)} \leq l(s) \leq \frac{\ddot{q}_{i\max}(s) - q_i''(s)u(s)}{q_i'(s)} \end{aligned} \tag{16}$$

Similarly, the constraint expression of the path jerk is shown in equation (17).

$$-\dddot{q}_{i\max}(s) \le 3q''(s)\ddot{s} + q'(s)\dddot{s} + q'''(s)\dot{s}^2 \le \dddot{q}_{i\max}(s) \tag{17}$$

Based on equation (17), the dimensionality of the variable remains unchanged when increasing the path jerk constraint variable $\dddot{s}$, and the convexity of the optimization problem remains unchanged to convert the path jerk constraints condition into the linear path acceleration constraints. The joint jerk constraint is established indirectly. Based on equation (8), the velocity relationship between two adjacent points is determined as follows by assuming that the motion between two adjacent discrete path points is uniformly accelerated or decelerated:

$$u^{n+1} = u^n + 2\Delta s^n l^n \qquad n = 1, 2, \ldots N-1 \tag{18}$$

where $\Delta s^n = s^{n+1} - s^n$, and n is the number of discrete path points.

According to equation (18), the velocity value can be calculated if the corresponding acceleration of each path point is known. The change in acceleration between two adjacent points is obtained as shown in equation (19).

$$\frac{d\ddot{s}}{ds} = \frac{d\ddot{s}}{dt}\frac{dt}{ds} = \frac{\dddot{s}}{\dot{s}} = \frac{\dot{l}(s)}{\sqrt{u(s)}} \tag{19}$$

where $\dot{l} = \dddot{s}$.

Based on equation (19), the change of acceleration between two discrete points is presented as follows.

$$\ddot{s}^{n+1} - \ddot{s}^n = \frac{2(s^{n+1} - s^n)\dddot{s}^n}{\sqrt{(\dot{s}^n)^2 + 2(s^{n+1} - s^n)\ddot{s}^n} + \sqrt{(\dot{s}^n)^2}} \tag{20}$$

According to equation (20), the linear acceleration constraint expression with the path jerk extreme value can be obtained as

$$\ddot{s}^n + \frac{2\Delta s^n \dddot{s}_{\min}}{\sqrt{(\dot{s}^{n+1/2})^2 + 2\Delta s^n \ddot{s}^n} + \sqrt{(\dot{s}^{n+1/2})^2}} \le \ddot{s}^{n+1} \le \ddot{s}^n + \frac{2\Delta s^n \dddot{s}_{\max}}{\sqrt{(\dot{s}^{n+1/2})^2 + 2\Delta s^n \ddot{s}^n} + \sqrt{(\dot{s}^{n+1/2})^2}} \tag{21}$$

4. OPTIMAL TRAJECTORY PLANNING

This study uses the interior-point method to solve the convex optimization model of time–energy optimal trajectory planning. The optimization problem becomes the large-scale sparse problem by introducing the pseudo-path parameter s, pseudo-velocity square $\dot{s}^2$, and pseudo-acceleration $\ddot{s}$. The specific process is as follows. First, the given path is transformed into a parameter expression using the pseudo-path parameter s as a variable and $s \in [0,1]$. At a certain interval, s is discretized to generate discrete $N+1$ points and satisfy $0 = s^0 \le s^n \le 1 = s^N, n = 0, 1, \ldots, N$. Further, the corresponding discrete points $l^0 = l(s^0), l(s^1), \ldots, l^N = l(s^N)$, $u^0 = u(s^0), u(s^1), \ldots, u^N = u(s^N)$ and $\tau^0 = \tau(s^1), \tau(s^2), \ldots, \tau^N = \tau(s^N)$ can be obtained. Finally, $u(s)$, $l(s)$ and $\tau_i(s)$ are modeled to determine the optimal values of u^n, and τ_i^n that satisfy the objective function and constraints.

Assuming that the optimization variable $u(s)$ is a piecewise linear function, $l(s)$ is a piecewise linear constant and $\tau_i(s)$ is piecewise nonlinear, that is, for $s \in [s^n, s^{n+1}]$, the expression of $u(s)$ is

$$u(s) = u^n + \left(\frac{u^{n+1} - u^n}{s^{n+1} - s^n}\right)(s - s^n) \tag{22}$$

To estimate l^n and τ^n, we adopt the median value of the adjacent discrete points, that is, the value of $l^n = l(s^{n+1/2})$ and $\tau^n = \tau(s^{n+1/2})$ at $s^{n+1/2} = (s^n + s^{n+1})/2$, such that the optimized objective function may

be approximately expressed as

$$\begin{aligned}
&\min \int_0^1 [\frac{\eta_1}{\sqrt{u(s)}} + \frac{(1-\eta_1)}{\sqrt{u(s)}} (\sum_{i=1}^{3} \frac{\tau_i(s)^2}{\overline{\tau}_i^2})] ds \\
&= \sum_{n=0}^{N-1} \int_{s^n}^{s^{n+1}} [\frac{\eta_1}{\sqrt{u(s)}} + \frac{(1-\eta_1)}{\sqrt{u(s)}} (\sum_{i=1}^{3} \frac{\tau_i(s)^2}{\overline{\tau}_i^2})] ds \\
&\approx \sum_{n=0}^{N-1} [\eta_1 + (1-\eta_1)(\sum_{i=1}^{3} \frac{\tau_i(s)^2}{\overline{\tau}_i^2})] \int_{s^n}^{s^{n+1}} \frac{1}{\sqrt{u(s)}} ds
\end{aligned} \tag{23}$$

where $\overline{\tau}_i$ is the maximum torque of each joint, the value of which is introduced to make the objective function dimensionless.

Considering the singularity of the integral of $u(s)=0$ it is necessary to consider $1/\sqrt{u(s)}$. According to the linear expression of $u(s)$, substituting equation (22) into equation (23), the objective function is expressed as follows

$$\min \sum_{n=0}^{N-1} [\eta_1 + (1-\eta_1)(\sum_{i=1}^{3} \frac{\tau_i(s)^2}{\overline{\tau}_i^2})] \frac{2(s^{n+1}-s^n)}{\sqrt{u^{n+1}} + \sqrt{u^n}} \tag{24}$$

In summary, let $\Delta s^n = s^{n+1} - s^n$, obtain the objective function and constraint conditions in the discrete form

$$\min_{u(\bullet), l(\bullet), \boldsymbol{\tau}(\bullet)} f_n(u^n) = \sum_{n=0}^{N-1} \frac{2\Delta s^n (\eta_1 + (1-\eta_1) \sum_{i=1}^{3} (\tau_i^n)^2 / \overline{\tau}_i^2)}{\sqrt{u^{n+1}} + \sqrt{u^n}} \tag{25}$$

subject to

$$\begin{aligned}
&\boldsymbol{\tau}_i^n = \boldsymbol{m}_i(s^{n+1/2}) l^n + \boldsymbol{c}_i(s^{n+1/2}) u^{n+1/2} + \boldsymbol{g}_i(s^{n+1/2}), \\
&u^0 = \dot{s}_0^2 = 0, \quad u^N = \dot{s}_T^2 = 0, \\
&l^0 = \ddot{s}_0^2 = 0, \quad l^N = \ddot{s}_T^2 = 0, \\
&u^{n+1} - u^n = 2 l^n \Delta s^n, \\
&u^n \geq 0, u^N \geq 0, \\
&z_1(u^n) = u^n - (\dot{\boldsymbol{q}}_{i\max}(s))^2 / (\boldsymbol{q}'_i(s))^2 \leq 0, \\
&z_2(u^n) = \frac{-\ddot{\boldsymbol{q}}_{i\max}(s) - \boldsymbol{q}''_i(s) u(s)}{\boldsymbol{q}'_i(s)} - l^n(s) \leq 0, \\
&z_3(u^n) = l^n(s) - \frac{\ddot{\boldsymbol{q}}_{i\max}(s) - \boldsymbol{q}''_i(s) u(s)}{\boldsymbol{q}'_i(s)} \leq 0, \\
&z_4(u^n) = \ddot{s}^n + \frac{2\Delta s^n \dddot{s}_{\min}}{\sqrt{(\dot{s}^{n+1/2})^2 + 2\Delta s^n \ddot{s}^n} + \sqrt{(\dot{s}^{n+1/2})^2}} - \ddot{s}^{n+1} \leq 0, \\
&z_5(u^n) = \ddot{s}^{n+1} - \ddot{s}^n + \frac{2\Delta s^n \dddot{s}_{\max}}{\sqrt{(\dot{s}^{n+1/2})^2 + 2\Delta s^n \ddot{s}^n} + \sqrt{(\dot{s}^{n+1/2})^2}} \leq 0, \\
&z_6(u^n) = \boldsymbol{\tau}_i(s^{n+1/2}) - \boldsymbol{\tau}(s) \leq 0, \\
&z_7(u^n) = \boldsymbol{\tau}(s) - \boldsymbol{\tau}_i(s^{n+1/2}) \leq 0, \\
&n = 0, 1, ..., N-1 \\
&i = 1, 2, 3
\end{aligned} \tag{26}$$

where $f_0, f_1, ..., f_{N-1} : R^n \to R$ is the convex function, that is, any local optimal solution is also globally optimal. The interior-point method is used herein to find the optimization variables $u^n (n = 0.1, ..., N-1)$ that meet the optimization goals and constraints.

The inequality constraints in equation (26) are processed by using the obstacle method to construct the interior-point penalty function, and the problem is transformed into the convex optimization problem with only equality constraints. The optimization goal is transformed into the following:

$$\min_{u(\bullet),l(\bullet),\tau(\bullet)} f_n(u^n)+\sum_{n=0}^{N-1}-(1/\gamma)\log(-\boldsymbol{z}_h(u^n)) \tag{27}$$

subject to

$$\begin{aligned}
&\tau_i^{\,n}=\boldsymbol{m}_i(s^{n+1/2})l^n+\boldsymbol{c}_i(s^{n+1/2})u^{n+1/2}+\boldsymbol{g}_i(s^{n+1/2}),\\
&u^0=\dot{s}_0^2=0,\quad u^N=\dot{s}_T^2=0,\\
&l^0=\ddot{s}_0^2=0,\quad l^N=\ddot{s}_T^2=0,\\
&u^{n+1}-u^n=2l^n\Delta s^n,
\end{aligned} \tag{28}$$

where $\boldsymbol{z}_h(u^n)=[z_1(u^n),z_2(u^n),....,z_7(u^n)]^T$. $f_n(u^n)$ and $\boldsymbol{z}_h(u^n)$ remain as defined in equations (25-26). For convenience, define $\varphi(u^n)=\sum_{n=0}^{N-1}-(1/\gamma)\log(-\boldsymbol{z}_h(u^n))$ as a logarithmic barrier function with the following gradient and Hessian matrix:

$$\nabla\varphi(u^n)=\sum_{n=1}^{N-1}-\frac{1}{z_i(u^n)}\nabla z_i(u^n), \tag{29}$$

$$\nabla^2\varphi(u^n)=\sum_{n=1}^{N-1}\frac{1}{-z_i(u^n)}\nabla^2 z_i(u^n)+\sum_{n=1}^{N-1}\frac{1}{z_i(u^n)^2}\nabla z_i(u^n)\nabla z_i(u^n)^T. \tag{30}$$

The objective function of equation (27) is multiplied γ. The optimization goal is then obtained as follows

$$\min_{u(\bullet),l(\bullet),\tau(\bullet)} F(u^n)\Leftrightarrow\min_{u(\bullet),l(\bullet),\tau(\bullet)}\gamma f_n(u^n)+\varphi(u^n) \tag{31}$$

For any $\gamma>0$, the above optimization problem has a unique optimal solution $u^*(\gamma)$, and the set $\{u^*(\gamma)\}$ composed of optimal solutions is called the central path. The specific steps and flowchart of the interior-point method to solve the time–energy optimal problem are presented in the following.

1.Calculate the initial value $\boldsymbol{u}^0=(\dot{s}^n)^2\approx[\frac{\Delta s^n}{\Delta w^n}]^2$, where $\Delta s^n=s^{n+1}-s^n$, $\Delta w^n=\max\left|(P^{n+1}-P^n)/\dot{q}_{i\max}\right|$, and make $z_i(u^0)<0$, $i=1,2,....,8$. Set $\sigma>0$, $\varepsilon\geq 0$, and $k=0$.

2.Calculate d^k. $d^k=-[\nabla^2F_{t_k}(u^k)]^{-1}\nabla F_{t_k}(u^k)$. If $d^k\neq 0$, continue to Step 3; if $\left\|\nabla^2 f_n(u^k)\right\|<\varepsilon$, select stop; otherwise, $\sigma_k=10*\sigma_k$, and repeat Step 2.

3.Let $\alpha_k=1$. If u^k+d^k is an interior point, continue to Step 4. Find $1\geq\bar{\alpha}_k>0$, such that u^k+d^k lies at the boundary of the feasible region, and return to Step 1.

4.Order $\alpha_k=0.9\bar{\alpha}_k$ and $u^{k+1}=u^k+\alpha_k d^k$. If $\sigma_k^{-1}\sum_{i=1}^{8}z_i(u^k)\leq\varepsilon$, stop the calculation; otherwise, if $\sigma_k=10\sigma_k$ and $k=k+1$, return to Step 2.

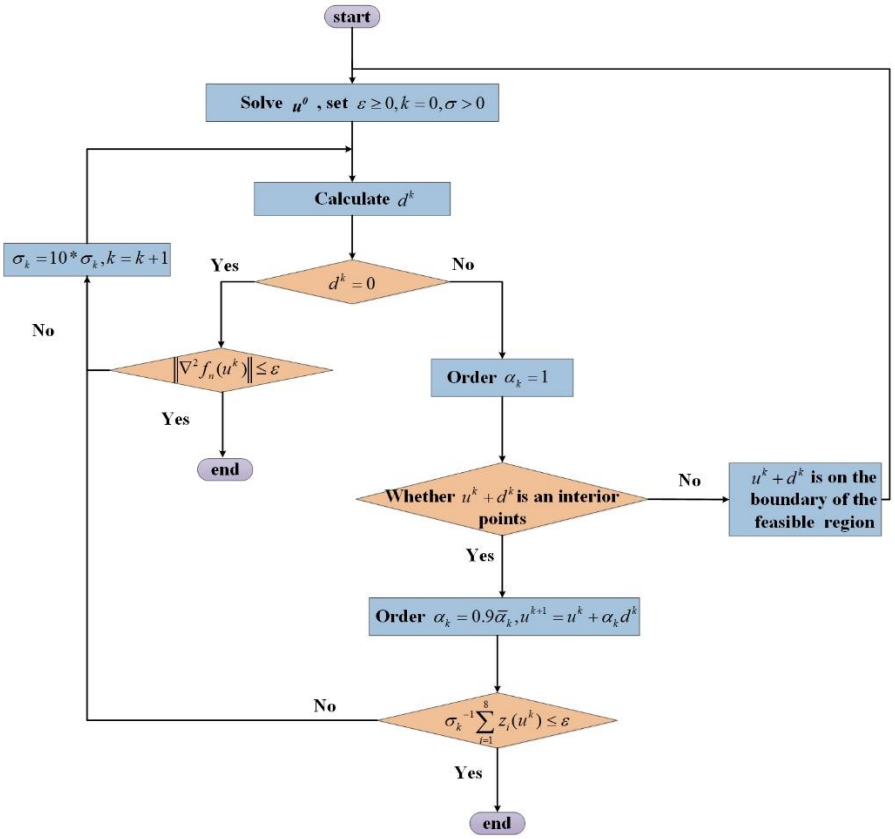

Figure 1. Time-energy optimal trajectory planning flow chart

Once the values of variable u^n are solved, the relational expression $s(t)$ representing the path coordinate axis and time can be obtained by solving $t(s)$. Then, the optimal motion curve of each joint that meets the performance indicators and constraints can be obtained.

5. EXPERIMENTS AND RESULT ANALYSES

To verify the effectiveness of the convex optimization model and the optimization algorithm, both are applied to the lifting material operation path of the PC1012 hydraulic excavator as shown in Figure 2. Table 1 presents the main working parameters of the excavator. Table 2 shows the relevant parameters of the excavator's dynamic model. Table 3 presents the velocity, acceleration, jerk, and torque constraints of each joint.

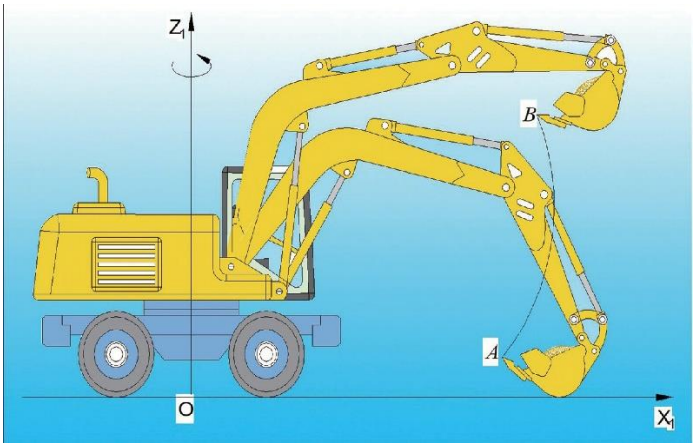

Figure 2. Secondary planning operation path of the PC1012 excavator.

Table 1 Main working parameters of PC1012 excavator

Parameters	Parameter value	Parameters	Parameter value
Bucket capacity ($\backslash m^3$)	0.049	Maximum digging depth ($\backslash m$)	1.6
Loaded material weight ($\backslash kg$)	88.2	Maximum digging height ($\backslash m$)	2.5
Maximum digging radius ($\backslash m$)	2.55	Maximum unloading height ($\backslash m$)	1.75

Table 2 Inertial parameters of the PC1012 excavator

Joint	Quality $\backslash kg$	Moment of inertia I_{izz} / $kg.m^2$	Centroid vector r / mm	Centroid angle α /°
Boom	42	23.2956123962	713.3807774	19.42
Arm	22	10.4469904262	310.0088159	6.02
Bucket	15	4.9048047417	211.7531224	38.38

Table 3 Physical constraints of the PC1012 excavator

Constraints	Boom joint	Arm joint	Bucket joint
Velocity (rad / s)	0.488	0.611	0.523
Acceleration (rad / s^2)	0.174	0.262	0.207
Jerk (rad / s^3)	0.174	0.174	0.174
Torque ($N.m$)	105	95	78

5.1 Time-energy optimal trajectory with different weight coefficients

To optimize the time-energy solution of the given hoisting path in Figure 2, first, take the total number of grid points of the discrete parameter s as $N = 1000$; second, use the inverse kinematics solution to convert the path points into a sequence of angle values of the boom, arm, and bucket joints; third, obtain the value of $q_i(s^n), q_i'(s^n), q_i''(s^n)$ using cubic spline to fit the discrete angle value of each joint ($i = 1, 2, 3$, $n = 1, 2, ...1000$); fourth, obtain the dynamic model of each joint using equation (5) (i.e., $m_i(s^n), c_i(s^n), g_i(s^n)$; and fifth, obtain the different weight coefficients time-energy trajectory by using the interior-point method for solving equations (25-26). Table 4 means the time and energy consumption of the excavator to lift the weight of 53, 70, and 79kg materials along the given path. Figure 3 depicts a comparison chart of the optimized values of time and energy consumption.

Table 4 presents the time–energy consumption optimal trajectory that satisfies the constraint conditions is obtained to lift the 53,70,79kg of the materials. And Figure 3 shows that (1) for the same quality of material, with an increase in the weight coefficient, the optimal energy consumption increases but the optimal time to complete the task decreases, i.e., when the focus is on low energy consumption, the efficiency of completing the task is reduced. Conversely, high-efficiency work requires high energy consumption. Therefore, in real-world engineering applications, appropriate weight coefficients should be selected according to the requirements of a task. In addition, for the same weight coefficient, as the material becomes heavier, the optimal time obtained via optimization is longer, and the energy consumption is higher. (2) Compared with the time and energy consumption value of skilled manual operation when completing the same target task, the secondary optimized trajectory showed higher efficiency and a lower energy loss, verifying the effectiveness of the planning method.

Table 4 Optimal time and energy consumption values

Material quality	Weight coefficient	Optimal time / *s*	Optimal energy consumption *kg / m*
53kg	Time-optimal trajectory $\eta_1 = 1$	12.532	95.637
	Time–energy optimal trajectory $\eta_1 = 0.5$	20.725	78.847
	Energy optimal trajectory $\eta_1 = 0$	28.247	65.625
	Before optimization	18.281	89.494
70 kg	Time-optimal trajectory $\eta_1 = 1$	15.673	102.735
	Time–energy optimal trajectory $\eta_1 = 0.5$	25.482	85.237
	Energy optimal trajectory $\eta_1 = 0$	32.763	72.253
	Before optimization	24.428	97.463
79 kg	Time-optimal trajectory $\eta_1 = 1$	18.531	112.634
	Time–energy optimal trajectory $\eta_1 = 0.5$ $\eta_1 = 0.5$	29.623	97.536
	Energy optimal trajectory $\eta_1 = 0$	37.372	81.534
	Before optimization	32.648	105.639

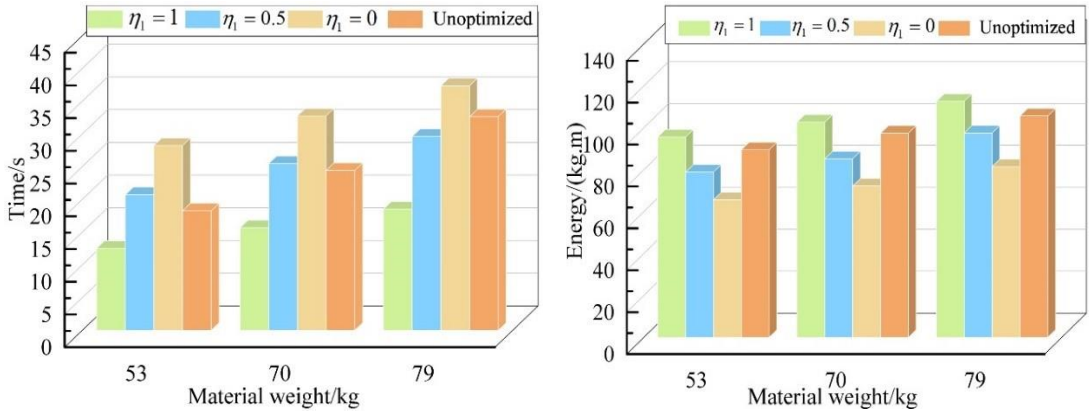

Figure. 3 Optimal time and energy consumption values with different weight coefficients

In addition, considering the effect of jerk on trajectory tracking accuracy and motion performance, the simulation results of lifting 70 kg materials at $\eta_1 = 0.5$ were compared with those of the second-order cone programming method proposed in [23] (where the jerk constraint limits were not considered) to verify the influence of the jerk constraint conditions on the joint velocity, acceleration, and torque performance. The results are shown in Figures 4-5. Table 5 presents the main comparison results of the joint jerk curves.

Figures 4-5 show that the movement time of the time–energy consumption optimal trajectory using the

second-order cone programming was 23.167s and that using our approach was 25.482s. Although the movement time was relatively long for our method, our planning method obtained smoother joint velocity, acceleration, and jerk curves, and the peak jerk, acceleration, and velocity reduced by 40.67%, 25.03%, and 12,54%, respectively, on average. This effectively suppressed the sudden change of acceleration, contributing to the smooth movement of the excavator and improving trajectory tracking accuracy. Therefore, from the perspective of actual working conditions, we consider the influence of jerk constraints in the operation process so that the excavator can show the best performance to complete the given task. The torque curves shown in Figure 6 indicate that the method proposed in this study can make the hydraulic driving device work in a stable manner, reduce the friction loss of each joint after increasing the jerk constraint conditions, protect the working device, and prolong the excavator's service life.

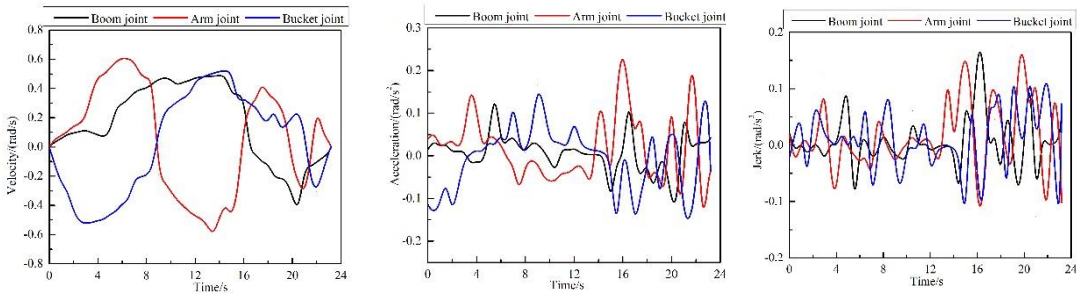

Figure. 4 Second-order cone programming algorithm: The joint velocity, acceleration, and jerk curves of the path points

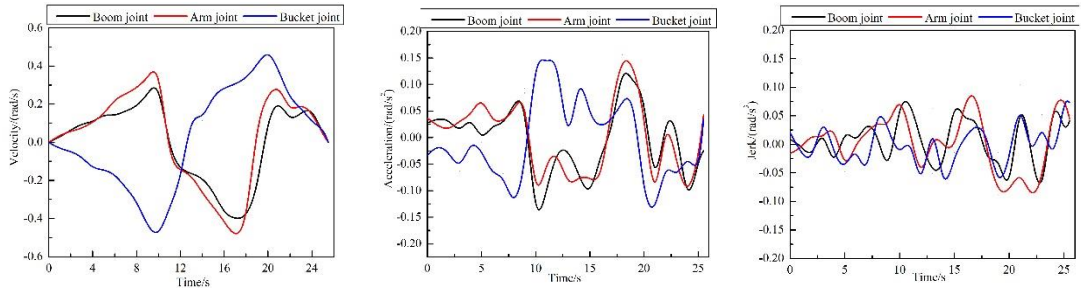

Figure. 5 Our planning algorithm: The joint velocity, acceleration, and jerk curves of the path points

Table 5 Comparison between the maximum value of the joint jerk curves.

	Boom joint	Arm joint	Bucket joint
Second-order cone programming algorithm (rad/s^3)	0.174	0.171	0.174
Interior-point method (rad/s^3)	0.113	0.098	0.097
Degree of decline (%)	35.06	42.69	44.25

Table 6 Comparison between the maximum value of the joint acceleration curves.

	Boom joint	Arm joint	Bucket joint
Second-order cone programming algorithm (rad/s^2)	0.163	0.262	0.207
Interior-point method (rad/s^2)	0.142	0.156	0.162
Degree of decline (%)	12.88	40.46	21.74

Table 7 Comparison between the maximum value of the joint velocity curves.

	Boom joint	Arm joint	Bucket joint
Second-order cone programming algorithm (*rad* / *s*)	0.488	0.603	0.523
Interior-point method (*rad* / *s*)	0.403	0.503	0.504
Degree of decline (%)	17.42	16.58	3.63

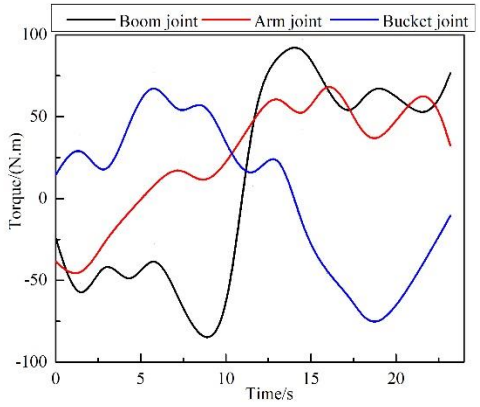

Torque curves of the second-order cone programming algorithm

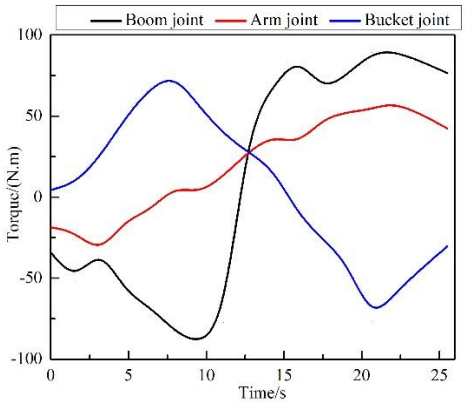

Torque curves of our planning method.

Figure. 6 Comparison chart of torque curves

5.2 Computational efficiencies with different algorithms

In practical applications, the time taken to determine the optimal performance index of the target path trajectory using the trajectory optimization algorithm is an important aspect of the calculation of the trajectory planning algorithm's efficiency. Therefore, the comparison and analysis of the interior-point method, genetic algorithm, and second-order cone planning algorithm were performed for the time–energy consumption optimal trajectory to determine the performance of the trajectory planning algorithm; the optimization efficiency results are presented in Table 8.

Table 8 shows that the interior-point method has certain advantages in determining the calculation efficiency compared with the second-order cone programming algorithm and the genetic algorithm. Moreover, the size of the optimization target weight coefficient affected the calculation efficiency of the trajectory planning algorithm. When time and energy consumption are considered at the same time, the time required for planning optimal trajectory increases.

Table 8 Comparison of the calculation efficiency of the optimized algorithms

Algorithm / Weight coefficient	Our approach	Genetic algorithm	Second-order cone programming
Time-optimal trajectory $\eta_1 = 1$	1.489s	8.691s	2.418s
Time–energy optimal trajectory $\eta_1 = 0.5$	2.136s	10.705s	3.105s
Energy optimal trajectory $\eta_1 = 0$	1.871s	10.14s	2.946s

6. CONCLUSIONS

This study selected the lifting path of an excavator as the optimization goal, established a time–energy consumption convex optimization model, and used the interior-point method to optimize the motion curves of the boom, arm, and bucket under the constraints of kinematics and dynamics models. First, considering the bucket when lifting materials of different qualities, the optimal trajectory of each joint with different weight coefficients was obtained and compared with the efficiency and energy consumption occurring during manual operation. These experimental results demonstrated that the trajectory obtained post-secondary optimization exhibited higher efficiency and reduced energy loss than that before optimization. Furthermore, the movement of each joint was more stable, avoiding sudden changes in the working process, protecting the hydraulic driving device, and achieving the high efficiency of the excavator, thereby verifying the effectiveness and feasibility of this method. Second, considering the optimization efficiency, our planning method, genetic algorithm, and second-order cone programming algorithm were used to obtain the time–energy optimal trajectory under different weight coefficients. The results demonstrated that our planning algorithm has high computational efficiency and reduced computing cost and optimization time.

As the future research, we will conduct an experimental verification of the optimization results to achieve high efficiency, low energy consumption, and stable operation of the excavator in actual engineering applications.

AUTHOR CONTRIBUTIONS

Yunyue Zhang: Conceptualization, Investigation, Software, Methodology, Writing-original draft, Writing-original draft. Zhiyi Sun: Resources, Formal analysis, Methodology, Writing-original draft, Writing-review & editing, Validation. Qianlai Sun: Funding acquisition, Project administration, Validation, Writing-original draft, Writing-review & editing. Yin Wang: Funding acquisition, Visualization, Writing-original draft, Writing-review & editing.

ACKNOWLEDGMENTS

This work is supported by the Key Research and Development Plan of Shanxi Province (Grant No. 201903D121130), Taiyuan University of Science and Technology Scientific Research Initial Funding (TYUSTSRIF, Grant No.20192014), PhD research startup foundation of Taiyuan University of Science and Technology (Grant No.20202038), Graduate Education Innovation Project (Grant No.2021Y670) and Natural Science Foundation of Shanxi Province (Grant No.201901D111265).

CONFLICT OF INTEREST STATEMENT

There are no conflicts of interest regarding the publication of this paper.

DATA AVAILABILITY STATEMENT

The data used to support the findings of this study are included in the article.

REFERENCES

[1] Dong, G., Nan, Y., Jerry, L., et al.: Kinematic modeling and constraint analysis for robotic excavator operations in piling construction. Automat Constr. 126(4), 103666 (2021). DOI: 10.1016/j.autcon.2021.103666

[2] Dongik, S., Seunghoon, H., Jeakweon, H.: Lever control for position control of a typical excavator in joint space using a time delay control method. J Intell Robot Syst. 102(3), 1-16

(2021). DOI: 10.1007/s10846-021-01416-z
[3] Dominic, J., Simon, K., Martin, W., et al.: Heap-the autonomous walking excavator. Automat Constr. 129(28), 103783 (2021). DOI: 10.1016/j.autcon.2021.103783
[4] Jeonghwan, K., Dong-eun, L., Jongwon, S.: Task planning strategy and path similarity analysis for an autonomous excavator. Automat Constr. 112, 103108 (2020). DOI: 10.1016/j.autcon.2020.103108
[5] Hao, F., Wei, M., Chenbo, Y., et al.: Trajectory control of electro-hydraulic position servo system using improved PSO-PID controller. Automat Constr. 127(7), 103722 (2021). DOI: 10.1016/j.autcon.2021.103722
[6] Guangjun, L., Lei, Y., Di, W., et al.: Development and experimental investigation of an automatic control system for an excavator. Proc Inst Mech Eng C J Mech Eng Sci. 235(4), 758-773 (2021). DOI: 10.1177/0954406220936308
[7] Xin, J., Kaikang, C., Yang, Z., et al.: Simulation of hydraulic transplanting robot control system based on fuzzy PID controller. Measurement. 164, 108023 (2021). DOI: 10.1016/j.measurement.2020.108023
[8] Ntt, Vu.: Robust adaptive controller design for excavator arm. In: International Conference on Robotics and Automation (ICRA), pp. 293-300. IEEE, Singapore (2020).
[9] Guangqiu, Y., Fuying, H., Zhanfu, Li., et al.: Workspace description and simulation of a backhoe device for hydraulic excavators. Automat Constr. 119, 103325 (2020). DOI: 10.1016/j.autcon.2020.103325
[10] Xiaobang, W., Wei, S., Eryang, Li., et al.: Energy-minimum optimization of the intelligent excavating process for large cable shovel through trajectory planning. Struct Multidiscipl Optim. 58(5), 2219-2237 (2018). DOI: 10.1007/s00158-018-2011-6
[11] Junxen, H., Pengfei, H., Kaiyuan, W., et al.: Optimal time-jerk trajectory planning for industrial robots. Mech. Mach. Theory. 121, 530-544 (2018). DOI: 10.1016/j.mechmachtheory.2017.11.006
[12] Serdar, K.: Optimal trajectory generation algorithm for serial and parallel manipulators. Robot Comput Integr Manuf. 48, 219-232 (2017). DOI: 10.1016/j.rcim.2017.04.006
[13] Serdar, K.: Maximal dexterous trajectory generation and cubic spline optimization for fully planar parallel manipulators. Comput Electr Eng. 56, 634-647 (2016). DOI: 10.1016/j.compeleceng.2016.07.012
[14] Huashan, L., Xiaobo, L., Wenxiang, W.: Time-optimal and jerk-continuous trajectory planning for robot manipulators with kinematic constraints. Robot Comput Integr Manuf. 29(2), 309-317 (2013). DOI: 10.1016/j.rcim.2012.08.002
[15] Louis-Francis Y, T., LFY, Marc, A., Meysar, Z.: Development of a trajectory planning algorithm for a 4-DoF rockbreaker based on hydraulic flow rate limits. Trans Can Soc Mech Eng. 44(4), 501-510 (2020). DOI: 10.1139/tcsme-2019-0173
[16] Qiushi, B., Guoqiang, W., Yongpeng, W., et al.: Digging Trajectory Optimization for Cable Shovel Robotic Excavation based on a Multi-Objective Genetic Algorithm. Energies. 13(12), 3118 (2020). DOI: 10.3390/en13123118
[17] Singh, S., Leu, M.C.: Optimal trajectory generation for robotic manipulators using dynamic programming. J Dyn Syst Meas Control. 109(2), 88-96 (1987). DOI: 10.1115/1.3143842

[18] Dominik, K., Hubert, G., Andreas, M.: Nearly optimal path following with jerk and torque rate limits using dynamic programming. IEEE Trans Robot. 35(2), 1-8 (2019). DOI: 10.1109/TRO.2018.2880120
[19] Bobrow, J.E., Dubowsky, S., Gibson, J.S.: Time-optimal control of robotic manipulators along specified paths. Int J Rob Res. 4(3), 3-17 (1985). https://doi.org/10.1177/0278364985 0400301
[20] Kang, S., Mckay, N.: Minimum-time control of robotic manipulators with geometric path constraints. IEEE Trans Automatic Control. 30(6), 531-541 (1985). DOI: 10.1109/TAC.1985. 1104009
[21] Pfeiffer, F., Johanni, R.: A concept for manipulator trajectory planning. IEEE Journal of Robotics and Automation. 3(2), 115-123 (1987). DOI: 10.1109/JRA.1987. 1087090
[22] Peiyao, S., Xuebo, Z., Yongchun, F.: Complete and time-optimal path-constrained trajectory planning with torque and velocity constraints: Theory and applications. IEEE ASME Trans Mechatron. 23(2), 735-746 (2018). DOI: 10.1109/TMECH.2018.2810828
[23] Peiyao, S., Xuebo, Z., Yongchun, F.: Essential properties of numerical integration for time-optimal path-constrained trajectory planning. IEEE Robot Autom Lett. 2(2), 888-895 (2017). DOI: 10.1109/LRA.2017.2655580
[24] Yanjie, L., Le, L., Haijun, H., et al.: A Method of Energy-Optimal Trajectory Planning for Palletizing Robot. Math Probl Eng. 2017, 1-10 (2017). DOI: 10.1155/2017/5862457